mum. None of the cells expressing ΔRII-CFP responded with increased $[cAMP]_i$ above 30% of the maximum (Fig. 5E). These results indicate that only the GFP-tagged PKA anchored to AKAPs can efficiently sense the localized change in $[cAMP]_i$ induced by β-AR stimulation.

The hypothesis of compartments of high $[cAMP]_i$ in cardiac myocytes was formulated more than 20 years ago (*4, 22*), and restricted pools of cAMP appear to function in catecholamines-mediated control of cardiac Ca^{2+} channels (*13*). Our data provide direct evidence of microdomains of high cAMP and demonstrate that cAMP can act with a short range of about 1 μm.

References and Notes

1. T. Hunter, *Cell* **100**, 113 (2000).
2. J. S. Hayes, L. L. Brunton, S. E. Mayer, *J. Biol. Chem.* **255**, 5113 (1980).
3. J. S. Hayes, N. Bowling, K. L. King, G. B. Boder, *Biochem. Biophys. Acta* **714**, 136 (1982).
4. I. L. Buxton, L. L. Brunton, *J. Biol. Chem.* **258**, 10233 (1983).
5. S. F. Steinberg, L. L. Brunton, *Annu. Rev. Pharmacol. Toxicol.* **41**, 751 (2001).
6. D. M. F. Cooper, N. Mons, J. W. Karpen, *Nature* **374**, 421 (1995).
7. R. V. Schillace, J. D. Scott, *J. Clin. Invest.* **103**, 761 (1999).
8. M. A. Laflamme, P. L. Becker, *Am. J. Physiol.* **277**, H1841 (1999).
9. T. Gao *et al.*, *J. Biol. Chem.* **272**, 19401 (1977).
10. J. Yang, J. A. Drazba, D. G. Ferguson, M. A. Bond, *J. Cell Biol.* **142**, 511 (1998).
11. K. L. Dodge *et al.*, *EMBO J.* **20**, 1921 (2001).
12. B. J. Bacskai *et al.*, *Science* **260**, 222 (1993).
13. J. Jurevicius, R. Fischmeister, *Proc. Natl. Acad. Sci. U.S.A.* **93**, 295 (1996).
14. RII-CFP and C-YFP were generated by polymerase chain reaction (PCR) amplification of the cyan mutant and a pH-insensitive yellow mutant, respectively, of GFP (kindly provided by R. Tsien, University of California, San Diego, San Diego, CA), by using the forward primer 5′-TAACCAAGCTTATGGTGAGCAAGGGC-3′ and the reverse primer 5′-CGCGGATCCTTACTTGTTCAGCTC-3′. The amplification products were cloned in frame at the 3′-end of the PKA subunits in the constructs RII-EBFP (*15*) and C-S65T (*15*) in place of EBFP and S65T, respectively. Both chimeras were then cloned into pCDNA3 (Invitrogen) as Hind III/Xba I fragments. ΔRII-CFP was generated by Pst I digestion and religation of pCDNA3–RII-CFP. The in-frame ablation of the Pst I fragment results in the deletion of a polypeptide that spans amino acids 15 to 40 in the RII subunit.
15. M. Zaccolo *et al.*, *Nature Cell Biol.* **2**, 25 (2000).
16. Cardiac ventricular myocytes from 1- to 3-day-old Crl:(WI)BR-Wistar rats (Charles River Laboratories, Wilmington, MA) were prepared as described (*23*). Briefly, ventricular tissue was enzymatically dissociated and the resultant cell suspension was plated onto 24-mm glass coverslips coated with laminin (Roche) and cultured in Dulbecco's modified Eagle's medium (DMEM) supplemented with 10% horse serum (HS) and 5% newborn calf serum (NCS). After 24 hours of culture, the medium was changed with DMEM supplemented with 5% HS and 0.5% NCS, and cells were transiently transfected with FuGene 6 (Roche) as described (*15*). All experiments were performed 36 to 48 hours after transfection in HEPES-buffered saline supplemented with 1 g $liter^{-1}$ glucose. All experiments were carried out at 37°C, and all chemicals were analytical grade.
17. Imaging of transfected cells was performed on a Zeiss Axiovert 100TX equipped with a CCD camera (T.I.L.L. Photonics GmbH, Martinsried, Germany) (Polychrome IV, T.I.L.L. Photonics GmbH), a software-controlled monochromator on the excitation side, and a filter wheel on the emission side. For RII-CFP imaging, transfected cells were excited at 440 nm, and fluorescence emission was collected using a 480DF30 emission filter (the dichroic mirror used was a 455DRLP). For C-YFP imaging, the excitation wavelength was 500 nm, the dichroic mirror was 525DRLP, and the emission filter was 545RDF35. All dichroics and emission filters are from Omega Optical.
18. M. Zaccolo, T. Pozzan, unpublished results.
19. D. V. Carr, Z. E. Hausken, I. D. Fraser, R. E. Stofko-Hahn, J. D. Scott, *J. Biol. Chem.* **267**, 13376 (1992).
20. FRET changes were measured as changes in the 480 nm/545 nm emission intensity using the software TillvisION v3.3 (T.I.L.L. Photonics GmbH) from the fluorescence images collected at 480 nm and 545 nm upon excitation of the cell at 440 nm (the dichroic mirror was a 455DRLP). For ratio calculation the background fluorescence was subtracted from each image. The integration time was 50 to 100 ms.
21. Y. Li, C. S. Rubin, *J. Biol. Chem.* **270**, 1935 (1995).
22. L. L. Brunton, J. S. Hayes, S. E. Mayer, *Adv. Cyclic Nucleotide Res.* **14**, 391 (1981).
23. D. E. Dostal, K. N. Rothbhlum, M. I. Chernin, G. R. Coope, K. M. Baker, *Am. J. Physiol.* **263**, C838 (1992).

24. We thank R. Tsien and S. Taylor for helpful discussion, S. Taylor for providing the PKA-anchoring inhibitory peptide Ht31, C. Destro for plasmid construction, V. Robert for help with myocyte primary cultures and discussion, and G. Ronconi, M. Santato, F. Cocco, M. Mongillo, and V. Toffolo for technical assistance. This work was supported by grants from Telethon-Italy, from the Italian Association for Cancer Research (AIRC), from the European Community, from the Italian Minister of University and Scientific Research (MURST), from the CNR (Target Project Biotechnology), and from the Armenise Harvard Foundation. M.Z. is an Assistant Telethon Scientist.

17 January 2002; accepted 25 January 2002

Structural Basis of Gating by the Outer Membrane Transporter FecA

Andrew D. Ferguson,[1] Ranjan Chakraborty,[2,3] Barbara S. Smith,[1] Lothar Esser,[1,4] Dick van der Helm,[2,5] Johann Deisenhofer[1]*

Siderophore-mediated acquisition systems facilitate iron uptake. We present the crystallographic structure of the integral outer membrane receptor FecA from *Escherichia coli* with and without ferric citrate at 2.5 and 2.0 angstrom resolution. FecA is composed of three distinct domains: the barrel, plug, and NH_2-terminal extension. Binding of ferric citrate triggers a conformational change of the extracellular loops that close the external pocket of FecA. Ligand-induced allosteric transitions are propagated through the outer membrane by the plug domain, signaling the occupancy of the receptor in the periplasm. These data establish the structural basis of gating for receptors dependent on the cytoplasmic membrane protein TonB. By compiling available data for this family of receptors, we propose a mechanism for the energy-dependent transport of siderophores.

Despite its relative abundance in Earth's crust, iron is biologically unavailable in an oxidizing atmosphere because of the insolubility of ferric oxyhydroxide. In response to iron deficiency, most microbes secrete organic chelators called siderophores, which are designed to sequester ferric iron. The ability to acquire this metal is an important determinant of bacterial virulence. Most bacteria express a sophisticated repertoire of parallel iron acquisition systems (*1*), which underscores their biological importance and the clinical potential to exploit these pathways for combating multi–drug-resistant bacterial strains (*2*).

Regulatory mechanisms, responsive to both the internal and external iron concentration, control the transcription of genes involved in iron uptake (*3*). The ferric citrate uptake (*fec*) genes are responsible for the transport of ferric citrate from the external medium into the cytoplasm (*4–7*). Proteins required for each phase of these energy-dependent transport processes have defined functions and are localized to specific cell envelope compartments. Embedded within the outer membrane is FecA, which performs two mutually independent functions: It binds and transports ferric citrate, and it is required to initiate transcription of the *fecABCDE* transport operon but not the regulatory *fecIR* genes (*4–7*). Both siderophore transport and the initiation of transcription require the

[1]Howard Hughes Medical Institute and Department of Biochemistry, University of Texas Southwestern Medical Center, 5323 Harry Hines Boulevard, Dallas, TX 75390, USA. [2]Department of Chemistry and Biochemistry, University of Oklahoma, 620 Parrington Oval, Norman, OK 73019, USA. [3]Department of Health Sciences, College of Public and Allied Health, East Tennessee State University, Post Office Box 70673, Johnson City, TN 37614, USA. [4]Laboratory of Cell Biology, National Cancer Institute, National Institutes of Health, 37 Convent Drive, Bethesda, MD 20892, USA. [5]Department of Biochemistry and Microbiology, University of Victoria, Post Office Box 3055, Victoria, British Columbia V8W 3P6, Canada.

*To whom correspondence should be addressed. E-mail: johann.deisenhofer@utsouthwestern.edu

chemiosmotic potential of the cytoplasmic membrane as transduced by a complex composed of the proteins TonB, ExbB, and ExbD. However, transport is not required for the initiation of transcription; rather, siderophore binding to FecA initiates a signaling cascade from the cell surface, resulting in transcription in the cytoplasm (*4–7*). The transmembrane regulatory protein FecR activates the cytoplasmic sigma factor FecI to bind to the *fecA* promoter (*4–7*). We therefore sought to probe the molecular architecture of FecA and its role in siderophore-induced transcription.

The three-dimensional structures of unliganded FecA and its complex with dinuclear ferric citrate were determined at 2.0 and 2.5 Å resolution by x-ray crystallography using multiple anomalous dispersion (MAD) (Table 1) (*8, 9*). The crystal structure of full-length FecA (741 residues) is composed of three domains (Fig. 1, A and B) and has an overall topology similar to those of FhuA (*9–11*) and FepA (*9, 12*). A monomeric 22-stranded β barrel is formed by residues 222 to 741. In vivo, these antiparallel strands traverse the outer membrane. Adjacent strands are connected by solvent-accessible extracellular loops containing two α helices and three β strands; turns are oriented toward the periplasm. The position and length of these connecting segments are different for each receptor (*9*). When viewed along its axis, the barrel has ellipsoidal dimensions (35 Å by 47 Å) and is 65 Å in height, extending 30 Å above the external interface of the upper leaflet of the outer membrane. Two girdles of aromatic residues inscribe the membrane-embedded hydrophobic surface of the receptor.

The plug domain (residues 80 to 221) is located inside the barrel, comprising five helices, two β strands, and a mixed four-stranded β sheet that is tilted by about 45° with respect to the membrane plane (Fig. 1, A and B). FhuA and FepA present a similar fold (*9*). The plug domain prevents the direct passage of ferric citrate across the outer membrane and separates the external and periplasmic pockets, which are located above and below the four-stranded β sheet. The extracellular pocket of FecA is lined with positively charged residues (ferric citrate is negatively charged). The equivalent regions of FhuA and FepA are predominantly lined with aromatic and/or hydrophilic residues (*10–12*). The electrostatic properties of these pockets confer specificity on the basis of the chemical attributes of the siderophore. The flexible 79-residue domain of FecA termed the NH_2-terminal extension (residues 1 to 79), which resides entirely within the periplasm and transmits the liganded status of the receptor to FecR (*4–7*), was not visible in the electron density maps and could not be modeled.

Noncovalently bound within the external pocket of FecA is a single dinuclear ferric citrate molecule (*13*). Three loops of the plug domain—apices A (Thr[138]), B (Arg[155]), and C (Ser[180])—extend above the plane of the upper leaflet of the outer membrane. In the liganded structure, apices A, B, and C, to-

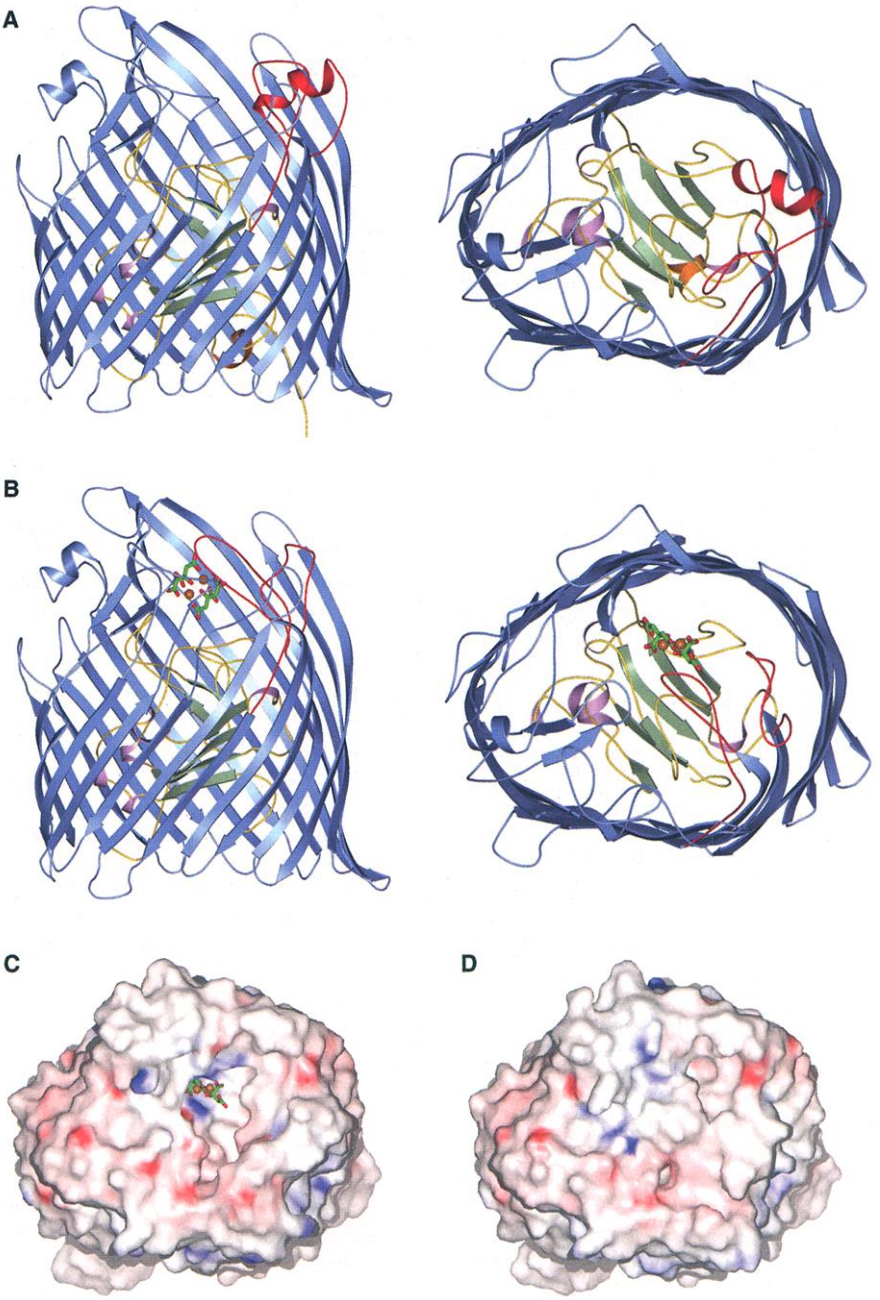

Fig. 1. Crystallographic structure of FecA, (**A**) unliganded and (**B**) liganded. The 22-stranded β barrel is shown in blue. The molecule is presented as found in the outer membrane with extracellular loops extending into the solvent (top) and periplasmic turns oriented toward the periplasm (bottom). Extracellular loops 7 and 8, which undergo major conformational changes upon ligand binding, are shown in red. The mixed four-stranded β sheet of the plug domain is shown in green, with helices in purple and loops in yellow. The switch helix, located in the periplasmic pocket of FecA, is colored orange and is only observed in the unliganded conformation. Dinuclear ferric citrate is represented as a bond model with oxygen atoms in red and carbon atoms in green; both ferric ions are shown as orange spheres. (**C**) Surface representation of unliganded FecA. Although ferric citrate is not found in the unliganded structure, it is represented as a bond model (with carbon atoms in green, oxygen atoms in red, and ferric ions in orange) to indicate the location of the binding site. (**D**) Surface representation of liganded FecA. The binding of ferric citrate causes conformational changes of the extracellular loops, such that the siderophore becomes solvent-inaccessible. The molecular surfaces are colored according to electrostatic potential, with blue and red corresponding to +40 kT and −40 kT, respectively. The view is given from the solvent. All figures were prepared using BobScript (*42*), GLR (*43*), POV-Ray, and GRASP (*44*).

gether with residues located on extracellular loops 4, 5, 8, and 11, form hydrogen bonds and electrostatic interactions with dinuclear ferric citrate (Fig. 2). Additional van der Waals contacts are provided by Leu^{156} from the plug domain and Phe^{333} from the barrel. The binding site of FhuA is markedly different from the binding site of FecA. Although apices A, B, and C of FhuA and several barrel residues also form specific interactions with the ligand, the binding site of FhuA is predominantly formed by hydrophobic residues (*10–12, 14, 15*).

Formation of the liganded complex substantially affects the conformation of the barrel and the plug domain of FecA. Binding of ferric citrate causes both minor and major changes in the spatial arrangement and conformation of five extracellular loops (Fig. 1, A and B). Minor changes (<0.5 Å) are observed in the fourth, fifth, and ninth extracellular loops. Strikingly, the seventh extracellular loop (residues 516 to 535) is translated by up to 11 Å, and it changes conformation such that helix 2 (residues 522 to 529) is unwound. Residues 562 to 581 from the eighth extracellular loop are also translated by up to 15 Å.

Allosteric transitions tightly regulate the opening and closing of TonB-dependent receptor channels, where these events are modulated by (i) siderophore binding and (ii) the transfer of stored potential energy from TonB. This bipartite gating mechanism refers to the process by which siderophore binding to its receptor induces allosteric transitions that enable transport by establishing or removing a physical channel obstruction, referred to as the gate (*16*). Opening and closing of the two gates regulates transmembrane siderophore flow. Diverse organisms, from bacteria to humans, use gating mechanisms in the regulated influx and efflux of solutes across biological membranes. The rearrangement of the seventh and eighth extracellular loops of FecA establishes the structural basis of gating for TonB-dependent receptors. In FecA, these movements render the external pocket and the ferric citrate-binding site inaccessible to solvent. Hence, the barrel of a TonB-dependent receptor is a dynamic entity that actively participates in the energy-dependent siderophore uptake (Fig. 1, C and D).

Allosteric transitions are propagated across the outer membrane by the plug domain via shifts (0.5 to 0.7 Å) toward the ferric citrate molecule of apices A and C, and of apex B away from the siderophore, and via the concerted downward movement (0.7 to 2.0 Å) toward the periplasm of βE and βF (*10, 11, 17*). In the liganded structure, an NH_2-terminal segment located within the periplasmic pocket of FecA, termed the switch helix (*10*), unwinds to assume a flexible extended conformation (as judged by the absence of interpretable electron density before residue Asn^{95}). Similar changes have been observed in the three-dimensional structures of multiple liganded complexes of FhuA (*10, 11, 14, 15*). The unwinding of the switch helix signals the occupancy of the receptor in the periplasm such that energized TonB molecules can effectively discriminate between unliganded and liganded receptors (*18*).

Table 1. Data collection, phasing, and refinement statistics.

Compound	Holo-native	Apo-native	Holo-selenomethionyl		Apo-selenomethionyl	
Space group	$P2_12_12$	$P2_12_12$	$P2_12_12$		$P2_12_12$	
Unit cell dimensions (Å)						
a	117.72	117.08	117.47		117.48	
b	89.36	88.09	88.76		88.25	
c	95.70	94.58	95.07		95.50	
$\alpha = \beta = \gamma$ (°)	90	90	90		90	
X-ray data						
Beam line	NSLS-X4A	NSLS-X12B	APS-BM19		APS-ID19	
Wavelength (Å)	1.73961	0.97800	1.00003	0.97951	0.97967	0.96411
Resolution range (Å)	50 to 2.8	50 to 2.0	50 to 2.5	50 to 2.5	50 to 2.5	50 to 2.5
Unique reflections	16,906	62,452	34,980	31,845	31,437	28,902
Average multiplicity	6.9	3.9	5.8	8.2	8.2	4.3
Completeness (%)	99.4	92.3	98.3	92.4	92.7	83.2
$\langle I/\sigma I \rangle$	13.1	11.1	6.6	22.6	22.6	13.8
R_{merge} (%)*	0.095	0.090	0.169	0.081	0.087	0.10
Phasing power	—	—	—	1.69	1.65	0.77
Figure of merit after SHARP refinement	—	—	—	—	0.4978	—
Figure of merit after density modification	—	—	—	—	0.8613	—

	Refinement	
	Liganded (holo-selenomethionyl)	Unliganded (apo-native)
R_{work}†/R_{free}‡ (%)	24.2/28.2	20.7/24.5
Ordered water molecules	252	368
Ordered LDAO§ molecules	16	17
Ordered heptane-(1,2,3)-triol molecules	0	2
Ordered dinuclear ferric citrate molecules	1	0
Root mean square deviation		
Bond lengths (Å)	0.007	0.011
Bond angles (°)	1.4	1.7
Average *B* factor (Å²)		
Protein	23.9	24.9
LDAO	44.9	70.9
Water	23.8	28.5
Heptane-(1,2,3)-triol	—	65.5
Ferric citrate	54.9	—

*$R_{merge} = \Sigma|\langle I_{hkl}\rangle - \langle I\rangle|/\Sigma\langle I_{hkl}\rangle$, where I_{hkl} is the integrated intensity of a given reflection. †$R_{work} = (\Sigma||F_{obs}| - |F_{calc}||)/(\Sigma|F_{obs}|)$, where F_{obs} and F_{calc} are observed and calculated structure factors. ‡For unliganded (apo-native) and liganded (holo-selenomethionyl) FecA, 5% of reflections were excluded from the refinement to calculate R_{free} (*8*). §LDAO: *N*,*N*-dimethyldodecylamine-*N*-oxide.

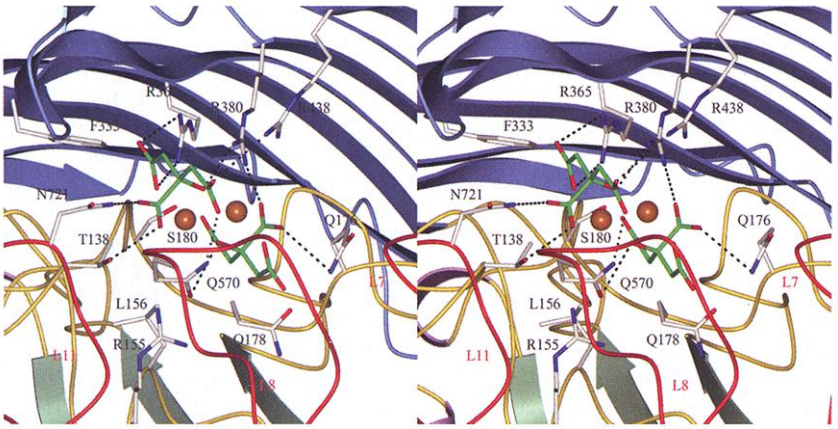

Fig. 2. Stereoview of the ferric citrate-binding site. All side chains within 3.5 Å of dinuclear ferric dicitrate are shown with carbon atoms in white, nitrogen atoms in blue, and oxygen atoms in red. Several water molecules found within the binding site mediate additional protein-ligand interactions. The strands and extracellular loops of the barrel are shown in blue; the strands forming the plug domain are in green, and loops are in yellow. The seventh, eighth, and eleventh extracelluar loops of the barrel are shown in red. The dinuclear ferric citrate molecule is represented as a bond model with oxygen atoms in red, carbon atoms in green, and ferric ions in orange.

The TonB-box is a functionally important region of TonB-dependent receptors (*19*) that physically interacts with TonB and is essential for the transfer of the chemiosmotic potential of the cytoplasmic membrane as transduced by the TonB-ExbB-ExbD complex (*20–23*). After ferric citrate binding, the TonB box of FecA (residues 80 to 84) becomes disordered, as evidenced by its lack of discernible electron density in the liganded structure.

By consolidating these data with other available genetic, biochemical, and structural observations for this family of TonB-dependent receptors, we have derived the following transport mechanism.

Stage 1: The siderophore is adsorbed from the medium with low affinity, primarily by aromatic residues found within the upper portion of the external pocket of the unliganded receptor.

Stage 2: The siderophore is transferred to its high-affinity binding site, where primarily apices A, B, and C of the plug domain and numerous charged residues found within the extracellular loops and β strands of the barrel form electrostatic contacts with the siderophore. These interactions cause translations of apices A, B, and C toward and away from the siderophore, as well as the concerted downward movement of other plug domain segments, leading to the unwinding and repositioning of the switch helix and the TonB-box.

Stage 3: Multiple extracellular loops of the receptor change their relative conformation and position. This bipartite gating mechanism closes the external pocket of the barrel, thereby favoring directed transport by disrupting the low-affinity binding site and shielding the high-affinity binding site from the solvent. However, the structural transitions observed in stages 2 and 3 may also be concerted.

Stage 4: Given the absence of an unobstructed channel of sufficient size to accommodate the passage of siderophores through TonB-dependent receptors, transitions that modify the conformation of the plug domain and/or barrel are required for transport. These changes are mediated by physical interactions between TonB and the TonB-box (*20–23*), and possibly by periplasmic turns of the barrel (*24*). Formation of a complex with TonB results in the transfer of stored potential energy to the receptor (*25*), which in turn promotes ligand transport.

Although the structural basis of the final energy-dependent transport stage remains to be established, two plausible models have been proposed (*10–12*). In the first proposal, an energized TonB molecule induces allosteric transitions within the plug domain and/or barrel, such that the unfolded plug domain with bound ligand is ejected into the periplasm. In the second proposal, the plug domain remains inside the barrel, and both domains undergo allosteric transitions that lead to the opening of an underlying transmembrane channel within the receptor, through which the siderophore permeates into the periplasm by a surface-diffusion mechanism (similar to those characterized for glycoporins). Biophysical studies recently revealed that in the absence of the FepA barrel, the plug domain is predominantly unfolded yet soluble and retains some binding affinity (*26*).

References and Notes

1. V. Braun, K. Hantke, W. Köster, in *Metal Ions in Biological Systems*, A. Sigel, H. Sigel, Eds. (Dekker, New York, 1998), pp. 67–145.
2. J. M. Roosenberg, Y. M. Lin, Y. Lu, M. J. Miller, *Curr. Med. Chem.* **7**, 159 (2000).
3. J. H. Crosa, *Microbiol. Mol. Biol. Rev.* **61**, 319 (1997).
4. C. Härle, I. Kim, A. Angerer, V. Braun, *EMBO J.* **14**, 1430 (1995).
5. M. Ochs *et al.*, *Mol. Microbiol.* **15**, 119 (1995).
6. I. Kim, A. Stiefel, S. Plantör, A. Angerer, V. Braun, *Mol. Microbiol.* **23**, 333 (1997).
7. A. Angerer, S. Enz, M. Ochs, V. Braun, *Mol. Microbiol.* **18**, 163 (1995).
8. Full-length FecA (pSV66) (*4*) was expressed using *E. coli* UT5600 and purified as described (*27*). Selenomethionyl FecA was obtained by growing these cells in the presence of seleno-L-methionine (60 mg/liter) as described (*28*) and purified in the presence of 5 mM dithiothreitol. Protein homogeneity and identity were assessed with SDS–polyacrylamide gel electrophoresis, dynamic light scattering, mass spectrometry, and Edman degradation. Well-ordered crystals of FecA were grown using the hanging-drop vapor diffusion technique with the use of crystal growth parameters as described (*27*). Crystals of FecA grew within 21 days, to a final size of 300 μm by 100 μm by 10 μm at 21°C, and exhibited a regular orthorhombic morphology. These crystals were mounted in cryoloops and flash-frozen by direct immersion into liquid propane. All diffraction data were collected at 100 K using a cryostream apparatus with synchrotron radiation from Argonne National Laboratory Structural Biology Center beam lines ID19 and BM19 at the Advanced Photon Source (supported by the U.S. Department of Energy, Office of Energy Research, under contract W-31-109-ENG-38) and beam lines X4A and X12B at the National Synchrotron Light Source, Brookhaven National Laboratory (supported by the U.S. Department of Energy, Division of Materials Sciences and Division of Chemical Sciences). All x-ray diffraction data were reduced with HKL2000 (*29*). These crystals have the symmetry of space group $P2_12_12$ with one molecule per asymmetric unit, and a Matthews coefficient V_m of 3.06 Å^3 per dalton (corresponding to a solvent content of 59%). Phase information was derived from MAD data collected from a single crystal measured at three wavelengths corresponding to the peak, inflection point, and high-energy remote of the selenium x-ray fluorescence spectrum (*30*). Of 14 selenium sites, 13 were located with Shake-and-Bake (*31*) and were refined with SHARP (*32*). Initial phases were improved by density modification and phase extension to 2.5 Å resolution using CNS (*33*). A structural model for unliganded FecA was built into the experimental electron density map with O (*34*) and refined with CNS. Dinuclear ferric citrate (*13*) and ferric citrate (Fluka) dissolved in water (2.5 mM) were soaked overnight into apo-FecA crystals. Refinement of both liganded data sets [FecA in complex with dinuclear ferric citrate (Table 1) or FecA in complex with ferric citrate (*35*)] revealed that the binding of either siderophore causes identical conformational changes. The liganded FecA structure was solved by molecular replacement using the unliganded structure as the search model. Nutrition assays demonstrate that dinuclear ferric citrate supports bacterial growth.
9. See supplemental material on *Science* Online at www.sciencemag.org/cgi/content/full/295/5560/1715/DC1.
10. A. D. Ferguson, E. Hofmann, J. W. Coulton, K. Diederichs, W. Welte, *Science* **282**, 2215 (1998).
11. K. P. Locher *et al.*, *Cell* **95**, 771 (1998).
12. S. K. Buchanan *et al.*, *Nature Struct. Biol.* **6**, 56 (1999).
13. I. Shweky, A. Bino, D. P. Goldberg, S. J. Lippard, *Inorg. Chem.* **33**, 5161 (1994).
14. A. D. Ferguson *et al.*, *Protein Sci.* **9**, 956 (2000).
15. A. D. Ferguson *et al.*, *Structure* **9**, 707 (2001).
16. Conformational changes in the conformation of the fourth extracellular loop of FhuA (*36–38*) and of the third and fourth extracellular loops of FepA (*39–41*) have been demonstrated by biophysical studies. Addition of ferric enterobactin shatters FepA crystals. The crystal structures of liganded FhuA also did not show changes in the conformations of the extracellular loops upon siderophore binding (*10, 11, 36, 37*). Inspection of the crystal packing arrangement of both FhuA crystal forms might provide an explanation for this apparent discrepancy. Contacts between symmetry-related FhuA molecules are primarily mediated by the fourth extracellular loop of the receptor, which has been shown to be involved in gating. These crystal contacts appear to favor an open-barrel conformation for FhuA. In contrast, the movements of

the extracellular loops of FecA are not restricted by crystal contacts. The absence of an altered β-barrel conformation upon siderophore binding may also reflect functional differences between FhuA and FecA or the regulation of the *fec* transport operon.
17. D. E. Koshland, *Nature Med.* **4**, 1112 (1998).
18. R. J. Kadner, K. J. Keller, *J. Bacteriol.* **177**, 4829 (1995).
19. E. Schramm, J. Mende, V. Braun, R. M. Kemp, *J. Bacteriol.* **169**, 3350 (1987).
20. N. Cadieux, R. J. Kadner, *Proc. Natl. Acad. Sci. U.S.A.* **96**, 10673 (1999).
21. N. Cadieux, C. Bradbeer, R. J. Kadner, *J. Bacteriol.* **182**, 5954 (2000).
22. G. S. Moeck, L. Letellier, *J. Bacteriol.* **183**, 2755 (2001).
23. G. S. Moeck, J. W. Coulton, K. Postle, *J. Biol. Chem.* **272**, 28391 (1997).
24. M. Braun, H. Killmann, V. Braun, *Mol. Microbiol.* **33**, 1037 (1999).
25. R. A. Larsen, M. G. Thomas, K. Postle, *Mol. Microbiol.* **31**, 1809 (1999).
26. K. C. Usher, E. Özkan, K. H. Gardner, J. Deisenhofer, *Proc. Natl. Acad. Sci. U.S.A.* **98**, 10676 (2001).
27. B. S. Smith *et al.*, *Acta Crystallogr.* **D54**, 697 (1998).
28. S. Doublié, *Methods Enzymol.* **276**, 532 (1997).
29. Z. Otwinowski, W. Minor, *Methods Enzymol.* **276**, 307 (1997).
30. W. A. Hendrickson, *Science* **254**, 51 (1991).
31. C. Weeks, R. Miller, *Acta Crystallogr.* **D55**, 492 (1999).
32. E. de La Fortelle, G. Bricogne, *Methods Enzymol.* **276**, 472 (1997).
33. A. T. Brünger *et al.*, *Acta Crystallogr.* **D54**, 905 (1998).
34. T. A. Jones, J.-Y. Zou, S. W. Cowan, M. Kjeldgaard, *Acta Crystallogr.* **A47**, 110 (1991).
35. A. D. Ferguson *et al.*, data not shown.
36. M. Bonhivers, A. Ghazi, P. Boulanger, L. Letellier, *EMBO J.* **15**, 1850 (1996).
37. L. Letellier, K. P. Locher, L. Plançon, J. Rosenbusch, *J. Biol. Chem.* **272**, 1448 (1997).
38. C. Bös, D. Lorenzen, V. Braun, *J. Bacteriol.* **180**, 605 (1998).
39. C. S. Klug, S. S. Eaton, G. R. Eaton, J. B. Feix, *Biochemistry* **37**, 9016 (1998).
40. D. C. Scott *et al.*, *J. Biol. Chem.* **276**, 13025 (2001).
41. X. Jiang *et al.*, *Science* **276**, 1261 (1997).
42. R. M. Esnouf, *Acta Crystallogr.* **D55**, 938 (1999).
43. L. Esser, personal communication.
44. A. Nicholls, K. A. Sharp, B. Honig, *Proteins Struct. Funct. Genet.* **11**, 282 (1991).
45. We thank N. Duke, S. Korolev, R. M. Sweet, and C. Ogata for their assistance during data collection; A. Bino for dinuclear ferric citrate; L. Venkatramani and E. Lemke for initial purification and crystallization experiments; Z. Otwinowski and W. Minor for sharing their data reduction expertise; and C. A. Brautigam, C. L. Colbert, E. Goldsmith, and D. Tomchick for critical reading of the manuscript. Supported by grants from the Welch Foundation (J.D.) and NIH (D.v.d.H.) and by postdoctoral fellowships from the Human Frontier Science Program and Canadian Institutes of Health Research (A.D.F.). Crystallographic coordinates and structure factor amplitudes have been deposited in the Protein Data Bank under the accession codes 1KMO (unliganded) and 1KMP (liganded).

22 October 2001; accepted 2 January 2002

Long-Range Interactions Within a Nonnative Protein

Judith Klein-Seetharaman,[1]* Maki Oikawa,[2] Shaun B. Grimshaw,[3] Julia Wirmer,[1]† Elke Duchardt,[1]† Tadashi Ueda,[2] Taiji Imoto,[2] Lorna J. Smith,[3] Christopher M. Dobson,[3]‡ Harald Schwalbe[1]†§

Protein folding and unfolding are coupled to a range of biological phenomena, from the regulation of cellular activity to the onset of neurodegenerative diseases. Defining the nature of the conformations sampled in nonnative proteins is crucial for understanding the origins of such phenomena. We have used a combination of nuclear magnetic resonance (NMR) spectroscopy and site-directed mutagenesis to study unfolded states of the protein lysozyme. Extensive clusters of hydrophobic structure exist within the wild-type protein even under strongly denaturing conditions. These clusters involve distinct regions of the sequence but are all disrupted by a single point mutation that replaced residue Trp^{62} with Gly located at the interface of the two major structural domains in the native state. Thus, nativelike structure in the denatured protein is stabilized by the involvement of Trp^{62} in nonnative and long-range interactions.

Incompletely folded states of proteins are coupled to cellular processes such as protein synthesis, translocation across membranes, and signal transduction [reviewed in (*1*, *2*)]. In addition, intrinsically unstructured proteins have been predicted to be common within the genomes of all organisms (*3*). Unstructured and partially folded conformations of proteins are, however, prone to aggregate and have been implicated in a wide range of diseases (*4*). The structural and dynamic characterization of nonnative states of proteins is therefore crucial for understanding these processes in addition to being fundamental to an understanding of protein folding itself.

Nonnative states of proteins are ensembles of conformers, the individual members of which may differ substantially in their structural and dynamic properties. Conformational sampling of denatured proteins can be significantly restricted, and the existence of "compact states" has been postulated to occur (*5*–*9*). In some cases, specific experimental structural information has been obtained although in general this information is either indirect or highly localized. An important question relating to all nonnative states is the extent to which long-range interactions are important in the stabilization of nonrandom interactions. We use site-directed mutagenesis and NMR spectroscopy to show that long-range nonnative interactions stabilize native-like hydrophobic clusters in lysozyme.

A wide range of approaches has been developed to characterize nonnative states of proteins in atomic detail by NMR spectroscopy (*10*), and evidence for the presence of residual structure even under strongly denaturing conditions has been presented, see, e.g. (*11*–*17*). Residual structure appears to reside predominantly in hydrophobic clusters, in which tryptophan or histidine residues are surrounded by other hydrophobic side chains (*18*–*20*). It has been postulated that hydrophobic clusters are stabilized by long-range interactions and may influence the folding of the protein, for example by acting as nucleation sites around which structure can be formed (*16*–*18*, *21*). Hydrophobic clusters have also been identified in nonnative states of hen lysozyme, in both the oxidized and the reduced form in 8 M urea at pH 2 [in the reduced protein the free sulfhydryl groups are blocked by methylation (*16*)].

Of the measured NMR parameters, chemical shift values of H^N and H_α protons and transverse (R_2) relaxation rates are the most direct indicators of residual structure. Here, we use such parameters to examine the reduced state of hen lysozyme in the absence of urea and then to investigate the structural changes resulting from the replacement of residue Trp^{62} by Gly (W62G). H^N and H_α chemical shifts measured for reduced and methylated wild-type lysozyme ($WT\text{-}S^{ME}$) in water are shown in Fig. 1A along with data for $WT\text{-}S^{ME}$ in 8 M urea (*16*). In $WT\text{-}S^{ME}$, significant deviations in chemical shifts of the H^N resonances from random coil values (*22*, *23*) can be seen for Gly^{22}, Trp^{63}, and Cys^{64}, and of the H_α resonances for residues 19 to 32, 58 to 64, 119 to 124, and 106 to 113. The largest differences are observed at positions 106 to 116, a result indicative of an increase in helical character for this region of

[1]Massachusetts Institute of Technology, Department of Chemistry, Francis Bitter Magnet Laboratory, 170 Albany Street, Cambridge, MA 02139, USA. [2]Graduate School of Pharmaceutical Sciences, Kyushu University, Fukuoka 812-8582, Japan. [3]Oxford Centre for Molecular Sciences, New Chemistry Laboratory, University of Oxford, South Parks Road, Oxford, OX1 3QH, UK.

*Present address: Institute for Software Research International, Carnegie Mellon University, Wean Hall 4604, Pittsburgh, PA 15213, USA.
†Present address: Johann Wolfgang Goethe-University, Center for Biological Magnetic Resonance, Institute for Organic Chemistry, Marie-Curie-Strasse 11, D-60439 Frankfurt am Main, Germany.
‡Present address: Department of Chemistry, University of Cambridge, Lensfield Road, Cambridge, CB2 1EW, UK.
§To whom correspondence should be addressed. E-mail: schwalbe@nmr.uni-frankfurt.de